Chapter 10

Finite-Element Modelling and Analysis of Hall Effect and Extraordinary Magnetoresistance Effect

Jian Sun and Jürgen Kosel

Additional information is available at the end of the chapter

http://dx.doi.org/10.5772/47777

1. Introduction

The Hall effect was discovered in 1879 by the American physicist Edwin Herbert Hall. It is a result of the Lorentz force, which a magnetic field exerts on moving charge carriers that constitute the electric current [1, 2]. Whether the current is a movement of holes, or electrons in the opposite direction, or a mixture of the two, the Lorentz force pushes the moving electric charge carriers in the same direction sideways at right angles to both the magnetic field and the direction of current flow. As a consequence, it produces a charge accumulation at the edges of the conductor orthogonal to the current flow, which, in turn, causes a differential voltage (the Hall voltage). This effect can be modeled by an anisotropic term added to the conductivity tensor of a nominally homogeneous and isotropic conductor.

The Hall effect is widely used in magnetic field measurements due to its simplicity and sensitivity [2]. Hall sensors are readily available from a number of different manufacturers and are used in various applications as, for example, rotating speed sensors (bicycle wheels, gear-teeth, automotive speedometers, and electronic ignition systems), fluid flow sensors, current sensors or pressure sensors.

Recently, a large dependence of the resistance on magnetic fields, the so-called extraordinary magnetoresistance (EMR), was found at room temperature in a certain kind of semiconductor/metal hybrid structure [3]. Sharing a similar origin with the Hall effect, the EMR effect is mainly based on the Lorentz force generated by a perpendicularly applied magnetic field, which causes a current deflection. This results in a redistribution of the current from the metal shunt into the semiconductor causing a resistance increase. It is important to note that the fundamental principle of EMR is the change of the current path in

the hybrid structure upon application of a magnetic field rather than the change of magnetoconductivity σ of either the semiconductor or the metal [4-5]. This effect has drawn much attention due to its potential advantages over other solid-state magnetic field sensors [6-9]. Noise is rather low in EMR devices, since they are made of nonmagnetic materials, and there is no contribution from magnetic noise as it is in contemporary tunnel magnetoresistance or giant magnetoresistance devices [10], and there is less thermal noise than in Hall sensors due to the lower resistance provided by the conducting shunt. The saturation field exceeds 1 T, resulting in a large working range and, compared to Hall sensors, EMR sensors provide a higher sensitivity.

EMR devices have been fabricated using high-mobility and narrow-gap semiconductors shunted by a highly conductive metal bulk [7]. These properties of the semiconductor guarantee that the material shows a large Lorentz force along with a comparatively good conductivity. Experiments on the EMR effect were initially performed in a macroscopic composite Van der Pauw disk made of a semiconductor disk with a concentric metallic circular inhomogeneity embedded (Figure 1(a)), and four electrodes were used to apply current and measure voltage. Though this structure provided good results, its realization in microscopic and nanoscopic length scales is unreasonable. Using bilinear transformation, a bar-type geometry, which is a semiconductor bar shunted by a metal stack on one side (Figure 1(b) and (c)), has been derived from the Van der Pauw disk showing a similar EMR effect and being simpler in terms of fabrication [11].

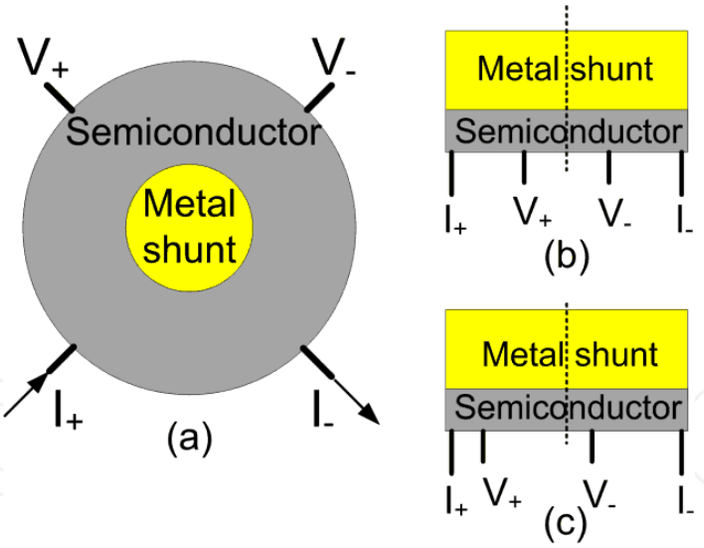

Figure 1. 4-contact EMR devices with (a) Van der Pauw disk geometry, (b) symmetric bar geometry and (c) asymmetric bar geometry. The dark lines labeled with I_+, I_- V_+ and V_- represent the two current electrodes and two voltage probes, respectively. The dashed lines represent the central axes of the devices.

The EMR effect is an extrinsic property that strongly depends on the geometry of the device and the placements of the electric contacts. Several studies have been carried out in order to investigate the influence of contact configurations and the geometry of the metallic region on the performance of the EMR device [12-14]. The typical 4-contact device consists of a high

mobility semiconductor bar with a metal shunt attached to one side. With respect to the placement of the two current electrodes (I) and the two voltage electrodes (V), two major kinds of four-contact configurations can be distinguished: IVVI (Figure (b) and (c)) and VIIV, where the voltage electrodes are between the current electrodes or vice versa, respectively.

Both the Hall and EMR effects are based on the Lorentz force, which can be considered by introducing an anisotropic conductive behavior in the material models. Depending on the characteristics of the materials being used and the complexity of the device geometry, the analytical calculation of the Hall and EMR effect can be very complicated. Several studies have shown that the finite element method (FEM) provides a proper tool to model and simulate the Hall and EMR effects.

In this chapter, we will introduce the 2-D and 3-D FEM models, which describe the anisotropic behavior of the conductors under an external magnetic field, and which can be applied to both Hall and EMR effects. Especially in case of the EMR effect, the 3-D simulations provide a considerably higher accuracy than the 2-D ones due to the inhomogeneous and unsymmetrical structures used. The developed 3-D model is also verified by experimental results. The models will be applied to study the effects of geometry on the performance of Hall and EMR devices. Thereby, the focus will be put on the EMR effect, since it has been much less investigated so far.

2. Theories of Hall and EMR effect

Both the Hall and EMR effects result in an anisotropic conductivity, which is caused by the magnetic field through the Lorentz force. The force acting on a single electric carrier can be expressed as

$$\boldsymbol{F} = \mathrm{q}(\boldsymbol{E} + (\boldsymbol{v} \times \boldsymbol{B})) \tag{1}$$

where $\boldsymbol{F}$ is the force vector acting on the charged carrier, q is the charge of the carrier, $\boldsymbol{E}$ is the vector of the applied electric field, $\boldsymbol{v}$ is the instantaneous drift velocity vector of the moving carrier and $\boldsymbol{B}$ is the magnetic field vector. The term $q\boldsymbol{E}$ is called the electric force, while the term $q\boldsymbol{v} \times \boldsymbol{B}$ is called the magnetic force $\boldsymbol{F}_m$.

In a solid conductor as shown in Figure 2, the current expressed in terms of the drift velocity is

$$I = \boldsymbol{j} \times A = nqvwd \tag{2}$$

where $\boldsymbol{j}$ is the current density and n is the number of charge carriers. The cross-section area of the conductor is $A = wd$, whereby w and d are the width and thickness of the conductor, respectively. Then the drift velocity is found as

$$\boldsymbol{v} = \frac{\boldsymbol{I}}{nqwd} \tag{3}$$

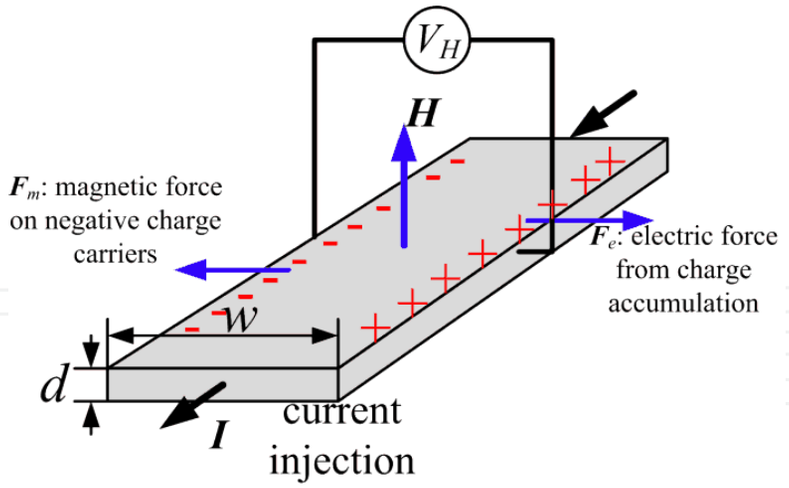

Figure 2. Schematic view of the bar (n-type) Hall device. A constant current, I, is applied as well as a constant magnetic field, H, perpendicular to the surface. This will cause an accumulation of charge carriers transverse to the current direction and a Hall voltage, V_H. F_m and F_e indicate magnetic force and electric force, respectively. Note that the direction of the current I in the diagram is that of conventional current, so that the motion of electrons is in the opposite direction.

When a magnetic field is applied in the direction perpendicular to the current flow, the Lorentz force causes deflection of the current. As a consequence, charges of opposite sign accumulate at two surfaces or edges of the conductor orthogonal to the current flow creating an electric field, the Hall field $\boldsymbol{E}_H$. When the magnetic force $\boldsymbol{F}_m$ is equivalent to the electric force $\boldsymbol{F}_e$ generated by the Hall electric field, an equilibrium state is achieved. In this case

$$\boldsymbol{F}_{\mathrm{m}} = \boldsymbol{F}_{\mathrm{e}} \Leftrightarrow q\boldsymbol{v} \times \boldsymbol{B} = \frac{V_H q}{w} \tag{4}$$

V_H is the output voltage caused by the electric field of the accumulated charges. Using equation (3) and (4), V_H can be expressed in terms of the applied current and the magnetic field

$$V_H = \frac{IB}{nqd} \tag{5}$$

For n-type semiconductors the charge carrier is negative (electron) and equation (5) can be substituted as

$$V_H = \frac{-IB}{ned} \tag{6}$$

where e is the electron charge.

In case of p-type semiconductors, V_H would, then, be positive for positive values of I and B. Another way of describing this is by means of the Hall angle, θ_H (Figure 3). The direction of the current is collinear with the applied electric field $\boldsymbol{E}$, but not collinear with the total electric field $\boldsymbol{E}_t$, because of the contribution from the Hall electric field $\boldsymbol{E}_H$. The angle between the total electric field and the applied electric field is called the Hall angle, θ_H,

$$\theta_{\mathrm{H}} = \arctan\left|\frac{E_{\mathrm{H}}}{j}\right| \tag{7}$$

and for small values it is approximated by

$$\theta_{\mathrm{H}} \approx \left|\frac{E_{\mathrm{H}}}{j}\right| \tag{8}$$

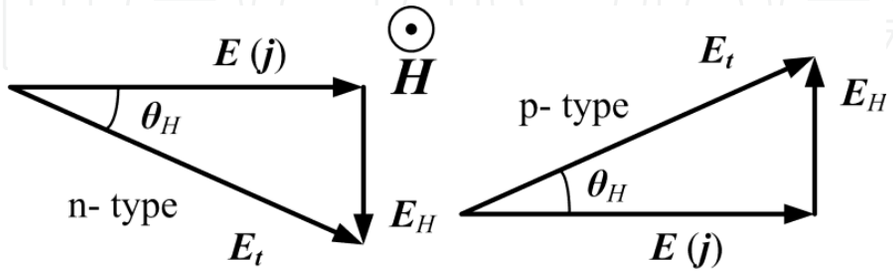

Figure 3. The Hall electric field E_H generated for n-type and p-type conductor based Hall devices. j is the current density, θ_H is the Hall angle indicating the difference between the applied electric field and the total electric field.

Let us suppose we have a semiconductor with a metal stack as an inhomogeneity embedded in it, as shown in Figure 4(a). The conductivities of the semiconductor and the metal are denoted as σ_s and σ_m, respectively, and $\sigma_m >> \sigma_s$. In low magnetic fields, the current flowing through the conductor is concentrated into the metallic region with the metal acting as a short circuit. The current density j is parallel to the total electric field E as indicated in Figure 4(a). The metal inhomogeneity is essentially an equipotential body due to its high conductivity. Thus, the direction of E at the semiconductor/metal interface is normal to the interface. At high magnetic fields, the current is deflected by the Lorentz force, which results in a directional difference between j and E by the Hall angle. For sufficiently high fields this angle approaches 90° in which case j is parallel to the semiconductor/metal interface and the current is deflected around the metal inhomogeneity which acts like an open circuit (Figure 4(b)). The transition of the metal from a short circuit at low fields to an open circuit at high fields gives rise to the very large magnetoresistance or the so-called extraordinary magnetoresistance effect.

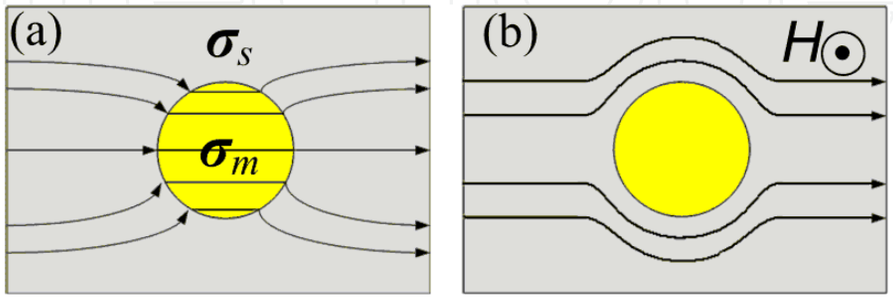

Figure 4. The current flow distribution in a semiconductor/metal hybrid. The gray and yellow areas express the semiconductor and metal, respectively. The dark lines show the paths of current. (a) At low magnetic fields, the current is parallel to the electric field E and the metal acts as a short circuit. (b) At high field, the current is mainly flowing in the semiconductor, the hybrid acts as an open circuit.

In the ideal case, the Hall effect is independent of geometry (compare equation (5) and (6)). However, the EMR effect is strongly geometry dependent, and analytical models for the EMR effect are highly complicated, especially when a complex geometry is considered. Therefore, the Finite Element Method (FEM) has been employed before to study the EMR effect [4, 14-16].

3. FEM models for Hall and EMR effect

The conductivity σ of a homogenous, isotropic solid conductor is given by

$$\sigma \equiv \frac{1}{\rho} = (n_e \mu_e + n_h \mu_h) q \tag{9}$$

where ρ is the resistivity, n_e and n_h are the densities of electrons and holes and μ_e and μ_h are the mobility of electrons and holes, respectively.

High sensitivity Hall and EMR devices are commonly made from n-type semiconductors since the mobility of electrons is typically much larger than that of holes yielding larger effects [17]. Therefore, only the dominant carrier-electron needs to be taken into consideration in the FEM model.

By direct integration of the Boltzmann equation [18], the current density due to carriers at a single quadratic energy extremum is given by

$$\boldsymbol{j} = \boldsymbol{\sigma}_0 (\boldsymbol{E} + \frac{\boldsymbol{j} \times \boldsymbol{H}}{n_e e}) \tag{10}$$

where $\boldsymbol{\sigma}_0 = n_e e \boldsymbol{\mu}$ is the conductivity without magnetic field, and $\boldsymbol{\mu}$ is the mobility tensor. In an isotropic conductor the mobility components are identical for all spatial axes

$$\boldsymbol{\mu} = \mu_e \begin{bmatrix} 1 & 0 & 0 \\ 0 & 1 & 0 \\ 0 & 0 & 1 \end{bmatrix} \tag{11}$$

According to Ohm's law, the vector of the current density is expressed as

$$\boldsymbol{j} = \boldsymbol{\sigma}(\boldsymbol{H}) \cdot \boldsymbol{E} \tag{12}$$

By re-arrangment of equation (10) into the form of equation (12), the magnetoconductivity tensor $\boldsymbol{\sigma}(\boldsymbol{H})$ is found to be

$$\boldsymbol{\sigma}(\boldsymbol{H}) = n_e e \left(\boldsymbol{\mu}^{-1} + \boldsymbol{H} \right)^{-1} \tag{13}$$

where $\boldsymbol{H}$ is a magnetic field matrix defined as

$$\boldsymbol{H} = \begin{bmatrix} 0 & -H_z & H_y \\ H_z & 0 & -H_x \\ -H_y & H_x & 0 \end{bmatrix} \tag{14}$$

H_x, H_y, and H_z are the components of the applied field in x-, y-, and z-directions, respectively. By substitution of equations (11) and (14) into equation (13), the components of the corresponding magnetoconductivity tensors are found to be

$$\begin{aligned}
\sigma_{11} &= (\mu_e{}^3 H_x{}^2 + \mu_e)p \\
\sigma_{12} &= \mu_e{}^2 (H_z + \mu_e H_x H_y)p \\
\sigma_{13} &= -\mu_e{}^2 (H_y - \mu_e H_x H_z)p \\
\sigma_{21} &= -\mu_e{}^2 (H_z - \mu_e H_x H_y)p \\
\sigma_{22} &= (\mu_e{}^3 H_y{}^2 + \mu_e)p \\
\sigma_{23} &= \mu_e{}^2 (H_x + \mu_e H_y H_z)p \\
\sigma_{31} &= \mu_e{}^2 (H_y + \mu_e H_x H_z)p \\
\sigma_{32} &= -\mu_e{}^2 (H_x - \mu_e H_y H_z)p \\
\sigma_{33} &= (\mu_e{}^3 H_z{}^2 + \mu_e)p \\
p &= n_e e(\mu_e{}^2 H_x{}^2 + \mu_e{}^2 H_y{}^2 + \mu_e{}^2 H_z{}^2 + 1)^{-1}
\end{aligned} \tag{15}$$

Since Hall and EMR devices are made of thin film structures, the thickness (z-direction) is typically neglected, and the complex 3-dimensional magnetoconductivity model is reduced to a concise 2-D model, where only the carrier transport in the x-y plane and a perpendicular magnetic field H_z are considered. By substituting x- and y-components of the magnetic field in equation (14) with zero, the magnetoconductivity of a 2-D model is found to be

$$\sigma(H) = \frac{\sigma_0}{1+\beta^2} \begin{bmatrix} 1 & -\beta & 0 \\ \beta & 1 & 0 \\ 0 & 0 & 1 \end{bmatrix} \tag{16}$$

where $\beta = \mu_e \cdot H_z$.

In a steady state condition, the problem of determining the electrostatic potential $\varphi(x,y,z)$ in the conductor reduces to the solution of a Laplace's equation:

$$\nabla\left[\boldsymbol{\sigma} \cdot \nabla\varphi(x,y,z)\right] = 0 \tag{17}$$

which can be solved by means of the finite-element method under specific boundary conditions and initial conditions [19].

4. Finite-element simulation of Hall effect

In this section, a cross-shaped hall device is investigated by means of the FEM using the 2-D model. The model of the Hall device consists of a semiconductor cross with the geometry shown in Figure 5. The dimensions of the 2 arms are 30×10 μm². The tips of the arms are

connected with narrow metal blocks acting as electric contact pads. The sensing area is defined by the intercross region of the two arms, which has an area of 10×10 μm². The material parameters are: μ_s = 4.55 $m^2V^{-1}s^{-1}$ and n_s = 2.55×10²² m^{-3} for the semiconductor; and μ_m = 5.3×10⁻³ $m^2V^{-1}s^{-1}$ and n_m = 5.9×10²⁸ m^{-3} for the metal (gold).

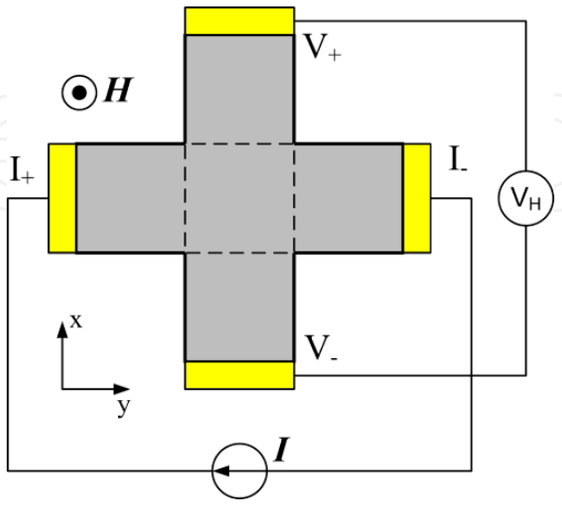

Figure 5. Schematic view of a cross-shaped Hall device. I_+, I_-, V_+, and V_- indicate the two current leads and two voltage probes, respectively.

A current of 100 μA is applied as boundary conditions at I_+ and I_- current pads, which is a feasible assumption based on the electromigration limit of Au as well as heating constraints. The I_- current pad is grounded. All other outer boundaries were set to electrical insulation (σ = 0, Neumann condition). The models were meshed with free triangular elements, which conform well to a large range of model geometries, and consisted of approximately 2.6×10⁴ elements and 5.3×10⁴ degrees of freedom. The electric potential along the device was obtained by solving equation (17). Figure 6 shows the potential distribution inside the device with and without application of a magnetic field. The Hall voltage is calculated as the

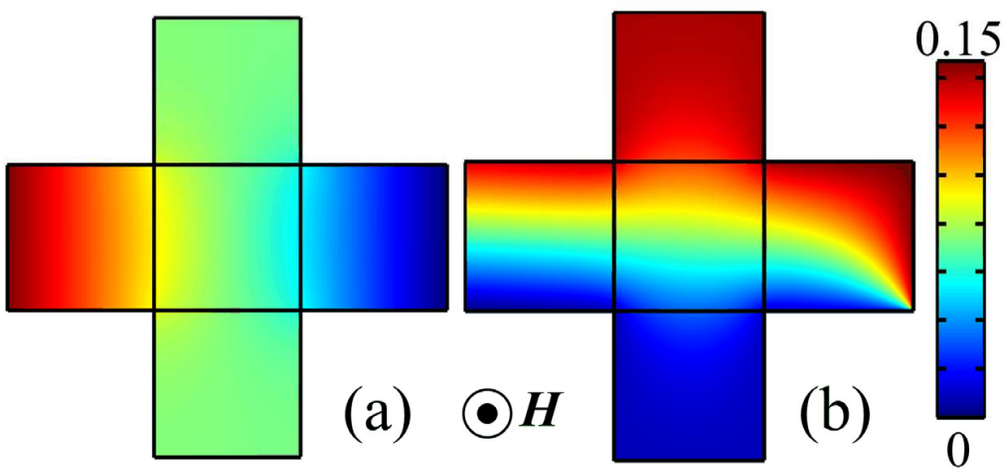

Figure 6. Potential distribution inside the Hall device (a) without and (b) with application of a magnetic field. The color bar indicates the strength of the voltage potential (V). The current flow is from the left to right side.

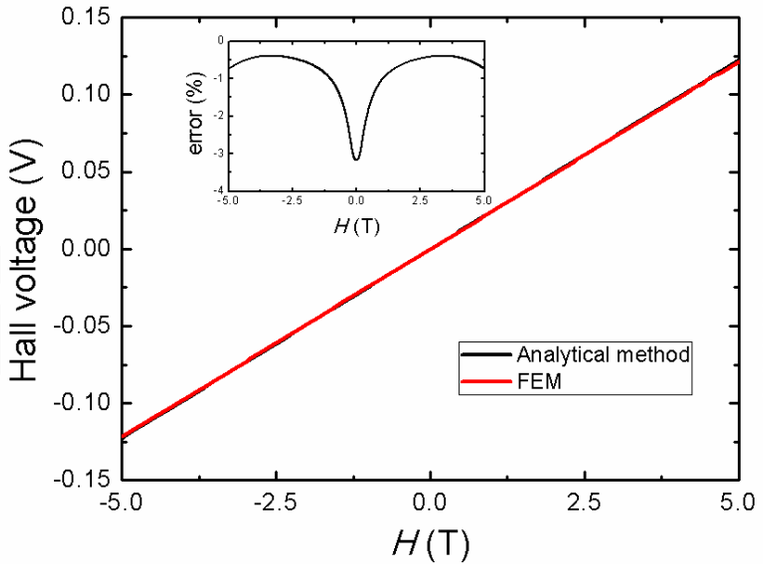

Figure 7. The Hall voltage as a function of the magnetic field calculated by an analytical and by FEM. The inset shows the error between the results from these two methods.

difference of the two potential values at voltage pads, i.e. $V_H = \varphi$ (V+) - φ (V-). Figure 7 shows the Hall voltage as a function of the magnetic field. The result from an analytical calculation is also provided for comparison. Within the magnetic field range of ±5 T, the analytical result is consistent with the one of the FEM showing a linear relation with the field change. The inset of Figure 7 shows the error between the results obtained with these two methods. The error is found to be only 1% to 3%, which shows the good agreement of the FEM with the analytical method.

5. Finite-element simulation of EMR effect

5.1. FEM simulation with 2-D model

In this section, a semiconductor/metal hybrid EMR device made of a semiconductor bar shunted by a concentric metallic inclusion (see Figure 4) is simulated with the 2-D FEM model in order to investigate the principle of the effect. The material parameters used in the simulation were the same as in section 3, i.e. $\mu_s = 4.55$ m^{2}V^{-1}s^{-1}, $n_s = 2.55\times10^{22}$ m^{-3}, $\mu_m = 5.3\times10^{-3}$ m^{2}V^{-1}s^{-1} and $n_m = 5.9\times10^{28}$ m^{-3}.

The device model consists of a semiconductor with an area of 100×100 μm^2 and a concentric metallic disk with a radius of 30 μm. A current density of 10^9 A/m^2 is applied to the left edge of the semiconductor as the boundary condition, and the right edge is grounded. All other outer boundaries were set to electrical insulation.

The current distributions in the semiconductor/metal hybrid device at various external magnetic fields are shown in Figure 8(a)-(d). At zero magnetic field (Figure 8(a)), the current flow is predominantly concentrated in the metal shunt, which can be seen clearly from the high current density in the metallic region and the low one above and below the disk in the semiconducting region. The electric field lines are perpendicular to the semiconductor/metal

interface and the current flow is parallel to the electric field lines. As the result, owing to the high conductivity of the metal, the current distribution at zero field constitutes the low resistance state of this structure.

As the external field rises to 0.1 T (Figure 8(b)), the current is still predominantly flowing through the metal shunt; however the magnetic field deflects the current path to some extent. Now, a larger proportion of the current is being forced to flow around the conductor through the semiconductor region of high resistance. Due to the current deflection, the direction of the electric field, which is still perpendicular to the surface of the metal shunt, and the one of the current are not parallel anymore and deviate from each other by the Hall angle.

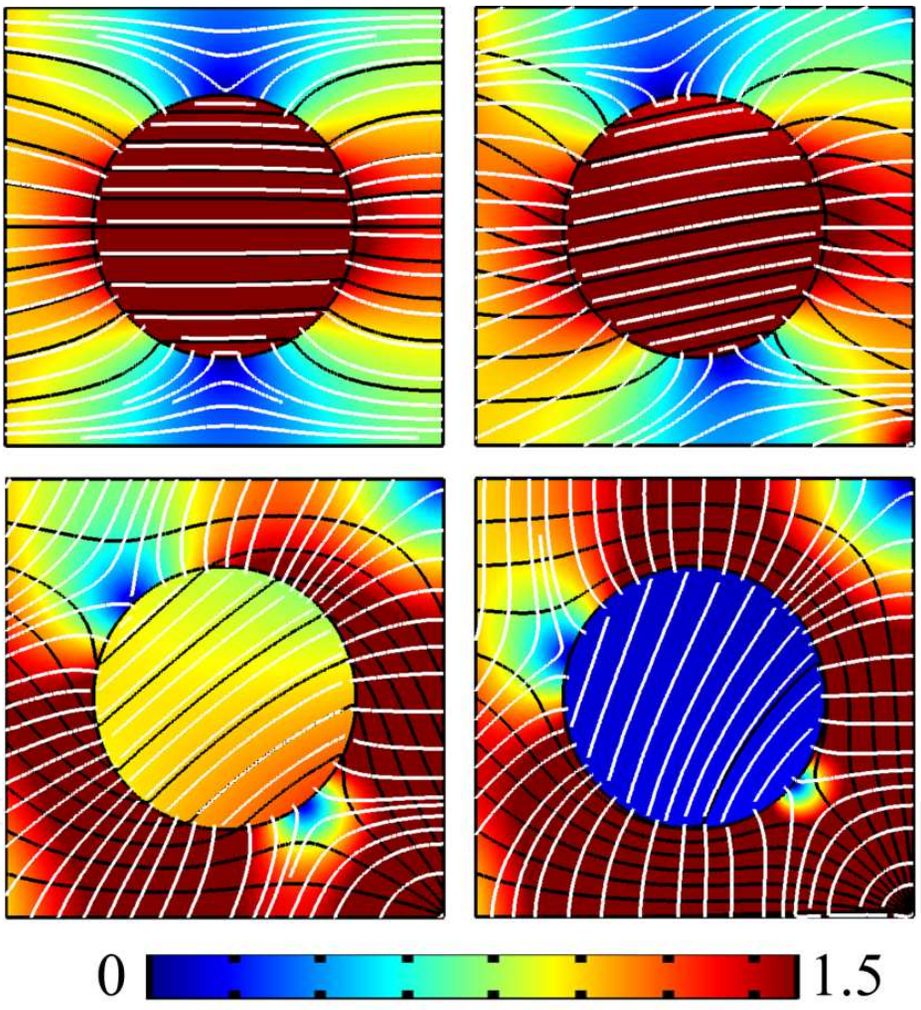

Figure 8. The current distributions in the semiconductor/metal hybrid device at external magnetic fields of (a) 0 T, (b) 0.1 T, (c) 0.5 T, and (d) 5 T. The dark solid lines indicate the paths of current. The white lines are the electric field lines. The color bar indicates the strength of the current density from 0 (blue) to 1.5×10^6 A/m^2 (red).

The Hall angle increases as the magnetic field becomes stronger. At 0.5 T (Figure 8(c)) highest current density is no longer observed in the metal region since the current is forced to flow through the semiconductor despite the higher resistance.

Finally, at a very strong applied field of 5 T (Figure 8(d)), he Hall angle approaches 90° forcing the current to flow almost entirely around the metal inhomogeneity. This results in a substantially higher resistance of the device compared to the case of no magnetic field applied.

5.2. FEM simulation with 3-D model

In this section, the EMR effect in a bar-type device is simulated under spatial magnetic fields with a 3-D FEM model.

In order to validate the simulation results, they are compared with experimental ones obtained from an EMR device specifically fabricated for this purpose. The EMR device consists of a semiconductor bar of 1.5 μm in thickness, 300 μm in length, and 23 μm in width (Figure 9). The metal shunt is a Ti (50 nm)/Au (250 nm) stack with a width of 80 μm. An overlap, which typically arises due to the fabrication process, of 3 μm exists between the semiconductor and metal shunt. Two metal leads with a length of 5 μm are located at the two corners of the semiconductor bar to apply the current and measure the voltage V. At the metal/semiconductor interface, the device showed a contact resistivity of 10^{-7} Ωcm², and this value was also implemented in the model.

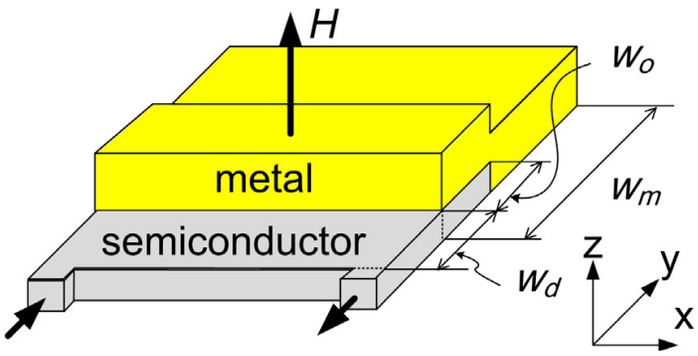

Figure 9. A bar-type EMR device with overlap between metal and semiconductor (typical for practical devices). The current injection direction is indicated by the solid arrows. The thickness of metal and semiconductor are denoted as t_m and t_s, respectively, and the width of metal and semiconductor are denoted as w_m and w_s, respectively. w_o represents the overlap between metal and semiconductor, note $w_d + w_o = w_s$.

A constant current with the density of 6.67×10^{7} A/m² (corresponding to 100 μA) was applied as the boundary conditions at the faces of the current leads. All other outer boundaries were set to be electrically insulating ($\sigma = 0$). The model was meshed with tetrahedral elements, whereby the mesh density was varied adaptively in order to account for the large differences of the dimensions of the structural components. The material parameters used in the simulation were the same as the ones of the experimental sample: $\mu_s = 0.82$ m²/V·s and $n_s = 5.6\times10^{22}$ m^{-3} for the semiconductor, $\mu = 5.30\times10^{-3}$ m²/V·s and $n = 5.90\times10^{28}$ m^{-3} for gold, and $\mu = 2.90\times10^{-3}$ m²/V·s and $n = 5.12\times10^{27}$ m^{-3} for titanium. Homogenous magnetic fields in x, y, and z direction changing from -1 to 1 T with steps of 0.1 T were applied. The result of a 2-D FEM simulation with a magnetic field applied in z-direction is also provided for

comparison, in which the width of the semiconductor is 20 μm and, due to the limitations of the 2-D model, only a gold shunt without a Ti adhesion layer is considered.

The EMR ratio, in general, is expressed as

$$MR(\boldsymbol{H}) = \frac{R(\boldsymbol{H}) - \mathrm{R}(0)}{R(0)},\ R(\boldsymbol{H}) = \frac{V(\boldsymbol{H})}{I} \tag{18}$$

where $R(\boldsymbol{H})$ is the resistance at spatial magnetic field $\boldsymbol{H}$ and $R(0)$ the resistance at zero magnetic field ($R(0) = R(\boldsymbol{H} = 0)$. $V(\boldsymbol{H})$ is the voltage at magnetic field $\boldsymbol{H}$ calculated from the solution of equation (17), and I is the value of current injected into the device. The output sensitivity δ is defined as the change of the output voltage with respect to a small variation $\Delta\boldsymbol{H}$ of the field

$$\delta(\boldsymbol{H}) = \frac{V(\boldsymbol{H} + \Delta\boldsymbol{H}) - V(\boldsymbol{H})}{\Delta\boldsymbol{H}} \tag{19}$$

In the case of the 2-D simulation, the magnetic field vector needs to be replaced by the perpendicular field component H_z in z-direction.

Figure 10 shows the simulated current paths in the EMR device as a function of external fields in different directions. (Note, different dimensions than the ones mentioned above are used for the device in order to provide clear illustrations). The dark streamlines show the current flow in the device. Without an external field, the current flows from the semiconductor into the metal, whereby a portion of the current flows through the overlap between the semiconductor and metal. As a magnetic field is applied, deflections of the current paths occur due to the Lorentz force. It is important to note that in case of magnetic fields applied in the x-direction (Figure 10 (a)), the current redistributions for positive and negative fields are asymmetric with respect to the current distribution at zero field, which is a result of the asymmetric geometry of the structure in x-view. However, in case of magnetic fields applied in z-direction or y-direction, current redistribution is symmetric.

Figure 11(a) shows the EMR ratio as a function of the perpendicular magnetic field H_z. Both the 2-D and 3-D FEM models provide accurate results for smaller field values. At higher fields the 3-D model is considerably more accurate than the 2-D model. For example, the EMR ratios at H_z = 1 T are 59.1%, 61.8%, and 76.2% from experimental measurement, 3-D FEM and 2-D FEM calculation, respectively. The larger EMR effect found with the 2-D simulation is mainly due to neglecting the lower conductivity of the titanium layer compared to gold and the semiconductor/metal overlap, which results in a wrong estimation of the device's resistance at zero field. The dependences of the EMR ratio to magnetic fields applied in planar directions are shown in Figure 11(b). The ratios are 11.5% and 8.2% at H_x = 1 T and 9.0% and 7.4 % at H_y = 1 T for experimental measurements and 3-D FEM calculations, respectively. Their values are about 15% to 20% of the ones obtained for a perpendicular field. A stronger EMR effect is observed at H_x than at H_y. This can be attributed to the difference in the strength of the Lorentz force acting on the carriers near the interface between the semiconductor and metal shunt, which is the region where the

Lorentz force has the largest impact on the current redistribution. The current density at the interface is highest near the source and drain contacts, where the current flow is mainly in y-direction. Therefore, the Lorentz force on the carriers at the interface is larger when the magnetic field is in x-direction rather than in y-direction. Also, the magnetoresistance curve for the fields in x-direction is asymmetric due to the asymmetric geometry.

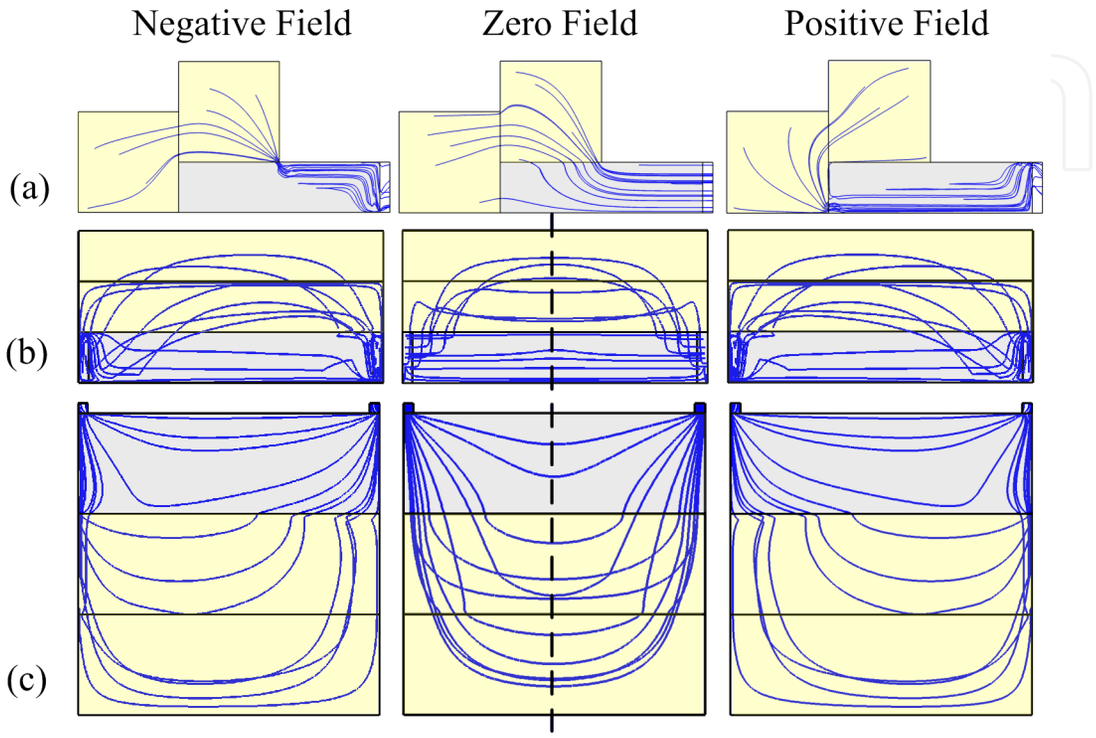

Figure 10. Current redistributions at magnetic field in (a) x-direction (left side view of Figure 9), (b) y-direction (front view of Figure 9), (c) z-direction (bottom view of Figure 9). The solid lines show the path of current flow. The yellow block represents the metal shunt and the grey block the semiconductor. ($t_m = 2t_s$, $w_m = w_s$, $w_o/ w_s = 50\%$).

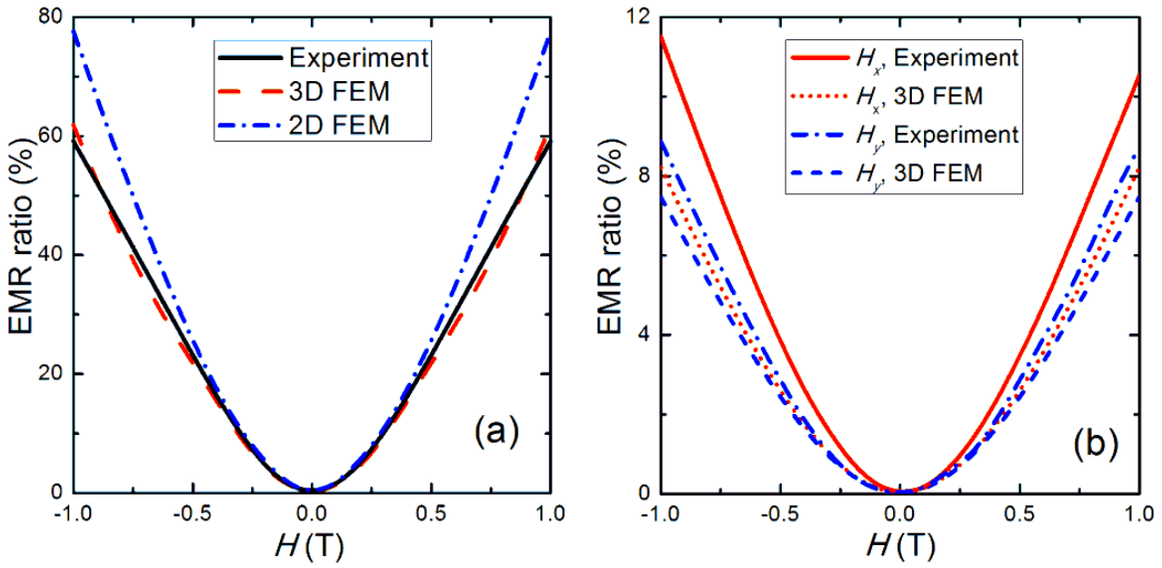

Figure 11. EMR ratios as functions of (a) perpendicular field H_z and (b) planar fields H_x and H_y.

The simulated results for planar fields are slightly smaller than the experimental ones. We assume this can be attributed to the defects in the semiconductor, which are more abundant in the vicinity of the interface. Since the current flow is not uniform in regions with defects, the current component in z-direction is larger as compared to the ideal case causing additional current redistribution due to Lorentz forces in case of planar fields.

6. FEM analyses on geometric dependence of EMR effect

As mentioned before, the EMR effect strongly depends on the geometry of the device and the locations of the electrodes. In this section, the performance of a bar-type EMR device is simulated for different device geometries and electrode locations. The performance is evaluated with regard to the output sensitivity (equation (19)) of the device, rather than the often-analyzed EMR ratio (equation (18)), since it is more relevant than the EMR effect for potential applications ranging from reading heads to smart biomedical sensors.

The model of the bar-type EMR device consists of a semiconductor bar shunted by a metal stack. The structure and geometric parameters of the device model are shown in Figure 12. The device is symmetric about the y-axis, and the x-axis is placed along one of the edges of the semiconductor. The widths of the semiconductor and metal and the lengths of the device are denoted W_s, W_m, and L, respectively. The current leads I and voltage probes V were placed along the edge of the semiconductor bar. Depending on their arrangement, the contact configuration can be classified into two types, namely, IVVI (Figure 12(a)) and VIIV (Figure 12(b)). While the two outer contacts are placed at the edges of the semiconductor, the locations of the inner ones are varied, whereby α_{VL}, α_{VR}, α_{IL} and α_{IR} are the distances of the left and right voltage probes and current leads in IVVI and VIIV configuration, respectively, from the y-axis.

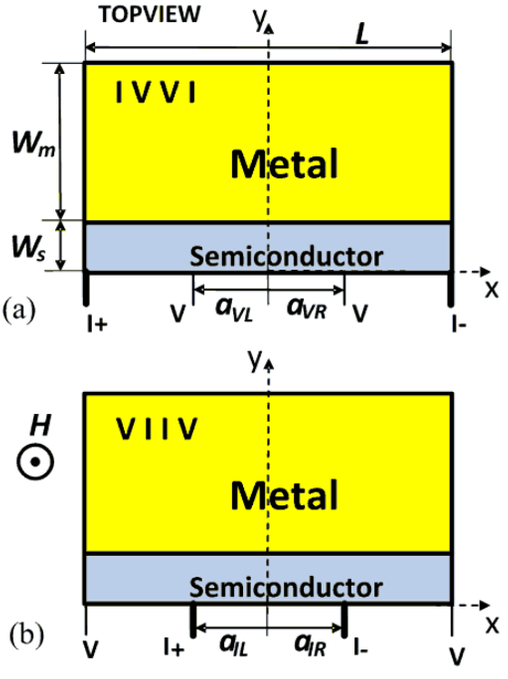

Figure 12. Geometry of the semiconductor/metal (a) IVVI and (b) VIIV configurations, where I and V represent current lead and voltage probe, respectively.

The material parameters are: $\mu_s = 4.55\ m^2V^{-1}s^{-1}$ and $n_s = 2.55\times10^{22}\ m^{-3}$ for the semiconductor, and $\mu_m = 5.3\times10^{-3}\ m^2V^{-1}s^{-1}$ and $n_m = 5.9\times10^{28}\ m^{-3}$ for the metal (300 K). The width W_m is 15 μm while W_s and L are varied during the simulation. A width of 0.1 μm is assigned to the current leads, while the voltage probes were considered as a point-like contact with zero width.

A current of 10 μA is applied as the boundary conditions at I_+ and I_-, which is a feasible assumption based on the electromigration limit of the metal as well as heating constraints. The current lead I_- is grounded. All other outer boundaries are electrically insulating ($\sigma = 0$, Neumann condition), while the interface between the semiconductor and metal is modeled with a contact resistivity of $10^{-8}\ \Omega\cdot cm^2$, which is a prerequisite for showing a strong EMR effect [15]. The models are meshed with free triangular elements, which conform well to a large range of model geometries, and consist of approximately 1.5×10^5 elements and 3×10^5 degrees of freedom. The mesh density is varied adaptively.

As pointed out before, the EMR effect and the output sensitivity of the device are strongly geometry dependent. Hence, the shape of the device and the placements of current leads and voltage probes are critical. We investigate the relationships between the output sensitivity and different semiconductor length/width ratios $\alpha = L/W_s$, the placements of the voltage probes in an IVVI configuration, and the placements of the current leads in a VIIV configuration as a function of the magnetic field. The output sensitivity is calculated using equation (19) with $\Delta H = 1\times10^{-4}$ T.

6.1. Width of the metal shunt

In this section, the influence of the width of the metal shunt is studied. An IVVI configuration is employed with a semiconductor of width $W_s = 5$ μm, length $L = 75$ μm, and symmetrically placed voltage probes with $\alpha_{VR} = -\alpha_{VL} = 12.5$ μm. The width of the metal shunt W_m is varied from $0.01\times W_s$ (50 nm) to $50\times W_s$ (250 μm). Figure 13 shows the sensitivity as a function of different W_m/W_s ratios at 0.05T and 1T. As can be seen, the sensitivity increases as the width of the shunt increases up to a certain value before it saturates. However, when W_m is thicker than $0.1\times W_s$, the influence is rather small with an increase of less than 1% for strong fields and around 3% for weak fields, indicating that the current is mainly confined to a thin layer in the metal shunt close to the semiconductor. Similar results were found for a model with a different semiconductor bar of $W_s = 3$ μm using the same values for all other parameters. Hence, it can be concluded that the dimension of the metal shunt should be larger than $0.1W_s$ in order to maintain a good performance of the EMR device. A thickness larger than $5W_s$ is not necessary due to its negligible influence on the device sensitivity. In the following simulations, a value of $W_m = 5W_s$ is being used.

6.2. Length/width ratio of the device

In order to investigate the influence of the length/width ratio α, a device with symmetric IVVI configuration is studied. The length L is varied from 30 μm to 105 μm with a step size of 3 μm in order to obtain different values of α, while W_s and α_{VR} are kept at 3μm and $L/6$,

respectively. The width of the metal is kept at $W_m = 5W_s = 15$ μm. Figure 14 shows the sensitivity as a function of α at magnetic fields of 0.05 T, 0.5 T, and 1 T. The optimum value of α with respect to sensitivity shows some dependence on the magnetic field. Values of 5, 10 and 20 provide maximum sensitivity for magnetic fields of 0.05, 0.5 and 1 T, respectively. The optimal value increases for stronger fields. This can be understood by the help of the insets in Figure 14, which indicate the relation between the length/width ratio and the current path in the EMR device. In very simplified terms, if no magnetic field is applied, the current flows straight through the semiconductor into the conductor shunt via the shortest possible way. Due to the Hall angle θ resulting from a magnetic field, the current path will be deflected into the semiconductor, which causes an increased resistance. It's important to keep in mind that a given external field will result in a certain Hall angle θ, independent of the geometry. In case of a low value α, the deflected current will be confined to the semiconductor bar (Figure 14 inset (a)). As α increases, the current path through the semiconductor becomes longer and, eventually, reaches the interface between the semiconductor and metal, leading to the optimal value of α, at which small changes of the magnetic field cause the largest changes in resistance (Figure 14 inset (b)). It can be seen from Figure 14 inset (c) that a further increase in length only increases the path of the current flow through the conductor, which doesn't contribute to the resistance. The sensitivity decreases as α increases. Since the Hall angle is larger at stronger fields, the optimal value of α is larger at stronger fields.

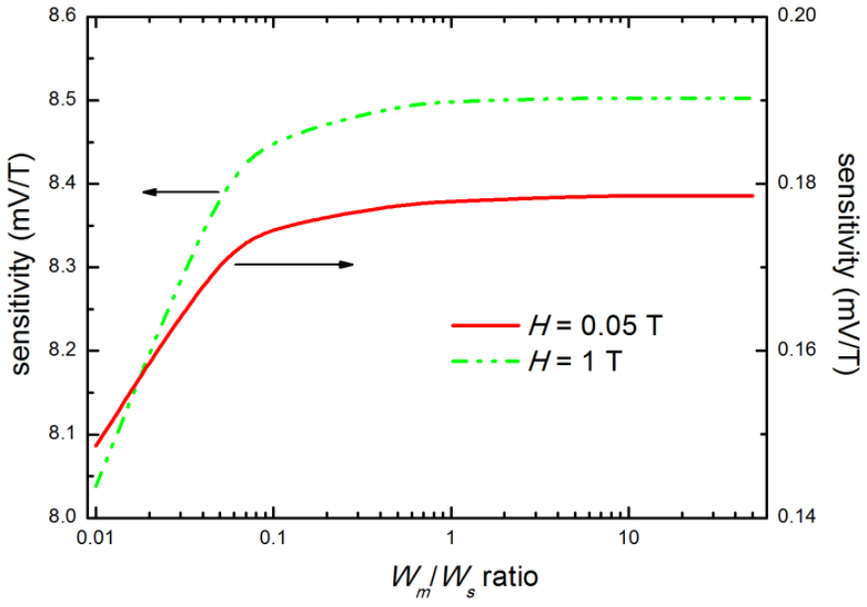

Figure 13. Output sensitivity of the EMR device as a function of the ratio W_m/W_s (W_s = 5 μm)at H = 0.05 and 1 T. The arrows indicate the corresponding axis.

The investigation of the length/width ratio is also carried out with a model of varied width W_s and fixed length L = 75μm. This simulation provided exactly the same results as the previous one indicating that the scale of a device has no influence on the performance of an EMR device. Therefore, EMR devices can be fabricated according to the spatial resolution requirements of the specific applications or restrictions due to the fabrication technology.

This not only gives flexibility with respect to design but also higher accuracy for specific applications.

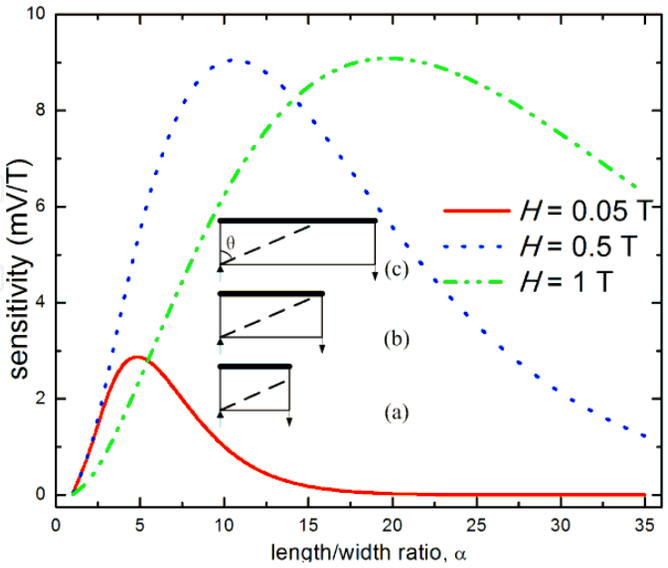

Figure 14. Sensitivity as a function of the length/width ratio α at various external fields. The insets show the current deflection in the semiconductor bar of the EMR device with (a) low length/width α, (b) optimal α, (c) large α under a constant Hall angle θ. The dashes indicate the deflected current path injected from the inlet current lead. The dark thick lines represent the interfaces between semiconductor and metal (not shown here).

6.3. Placement of voltage probes in IVVI configuration

An IVVI device with length L = 45 μm and width W = 3 μm (α = 15) is simulated to investigate the influence of the placement of the voltage probes. Here, α_V is used to denote the distance of the voltage probes from the y-axis (Figure 12 (a)). Firstly, a symmetric configuration is used, i.e. $\alpha_V = \alpha_{VL} = \alpha_{VR}$. α_V is changed from 0.5 to 22.5 μm in steps of 1 μm, and its influence on the sensitivity is shown in Figure 15. The sensitivity increases as the probes move further away from the y-axis at both weak and strong fields, and it can be concluded that the larger the separation of the probes the higher the performance. It is interesting to note that there is a considerable increase in sensitivity as the two probes approach their respective corners. In order to get a better understanding of this effect, Figure 16 shows the electric potential distribution along the edge of the semiconductor bar for different magnetic fields. Most of the potential change occurs in the semiconductor close to the current leads. This is due to the smaller cross-section available for the current to pass through, resulting in higher current densities and, consequently, larger electric fields. As the magnetic field increases, the current density along the right edge of the semiconductor increases even further, while on the left edge of the semiconductor the opposite happens (compare Figure 10(c) for positive fields). In between, the two edges, at higher fields, the amount of current flowing through the semiconductor increases thereby facing an increased resistance and, hence, larger potential differences are observed. Since the largest changes of the potential arise around the corners, higher sensitivity can be obtained by placing the

voltage probes closer to the corners (Figure 15). Hence, a symmetric EMR sensor with high sensitivity can be reduced to a two-contact device where the contacts are utilized for current injection as well as voltage measurement.

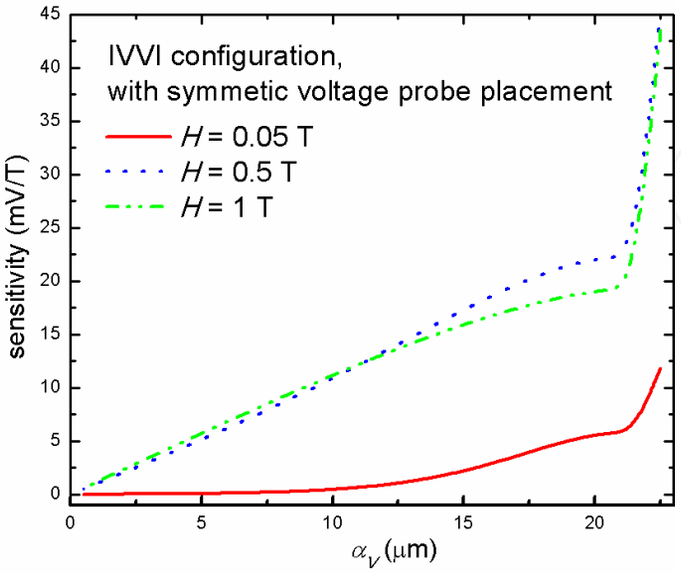

Figure 15. Sensitivity as function of the voltage probe placement at various external fields for the EMR device with symmetric IVVI configuration.

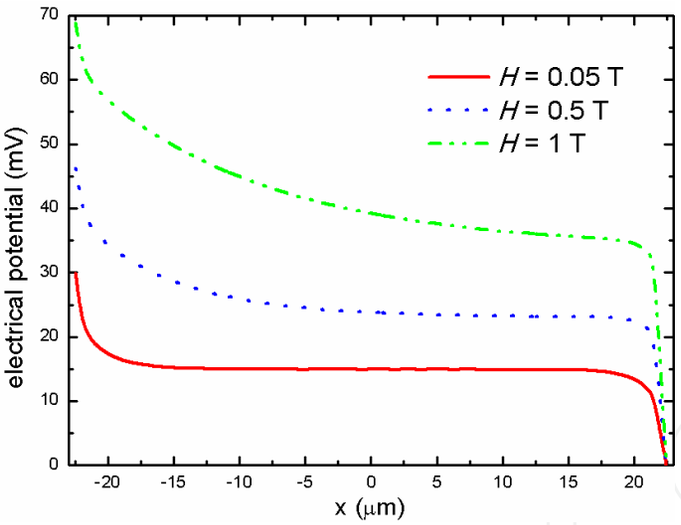

Figure 16. The potential distribution along the edge of the semiconductor bar in the EMR device at different magnetic fields.

It has previously been reported that an asymmetric contact configuration increases the EMR effect [12]. In order to study the influence of an asymmetric arrangement of the voltage probes, an IVVI configuration is simulated with α_{VR} fixed at 7.5 μm while α_{VL} is varied from -22.5 μm to 22.5 μm. The current is injected at the current lead with varying position. Figure 17 shows the sensitivity as a function of α_{VL}. Compared to the results found for the symmetric arrangement (Figure 15), the maximum sensitivity at high field (1 T) has reduced. In the case of low fields, the sensitivity has slightly increased due to the asymmetric arrangement.

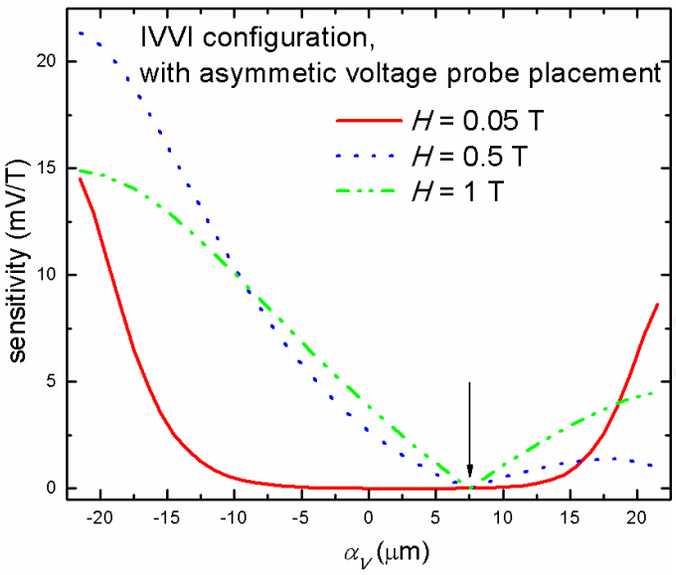

Figure 17. Sensitivity as a function of the placements of voltage probes at various external fields for the EMR device with asymmetric IVVI configuration. The arrow indicates the location of the fixed voltage probe.

6.4. Placement of current leads in VIIV configuration

The effect of the placements of the current leads α_I in a symmetric VIIV device is studied using the same geometric parameters for the model as before in section 5.3. α_I denotes the distance of the current leads from the device's center (Figure 12(b)). The sensitivity depends on α_I in a very similar way as it did on α_V in the case of the IVVI configuration and the same trends can be observed (Figure 18). Again, this result shows the high sensitivity that can be obtained by using a simple two-contact electrode arrangement. A study of asymmetric current lead arrangement shows that the sensitivity can only be improved for low magnetic fields (Figure 19), which is also similar to what is found for the asymmetric IVVI configuration. The large change in sensitivity as the leads are placed closer to the corners of the device can be explained in the same way as in case of the IVVI configuration. It can be concluded that VIIV and IVVI configurations are very similar in general and optimally utilized with two electrodes at the corners of the semiconductor.

7. Finite-element analysis on the effect of the semiconductor/metal interface

In this section, an IVVI bar-type EMR device is investigated. The geometry and dimensions of the device model are: W_m = 15 μm, W_s = 3 μm, L = 75 μm and α = 25 μm. The current leads (I_+, I_-) have a width of 0.1 μm. The voltage probes (V_1, V_2) are considered as a point-like contact. A current I of 100 μA is applied through setting the boundary condition of the current leads. At the semiconductor/metal interface, different values of the contact resistivity ρ between 10^{-11} Ω·cm^2 and 10^{-5} Ω·cm^2 are applied. In practice, 10^{-8} Ω·cm^2 is considered a very low ohmic contact resistivity.

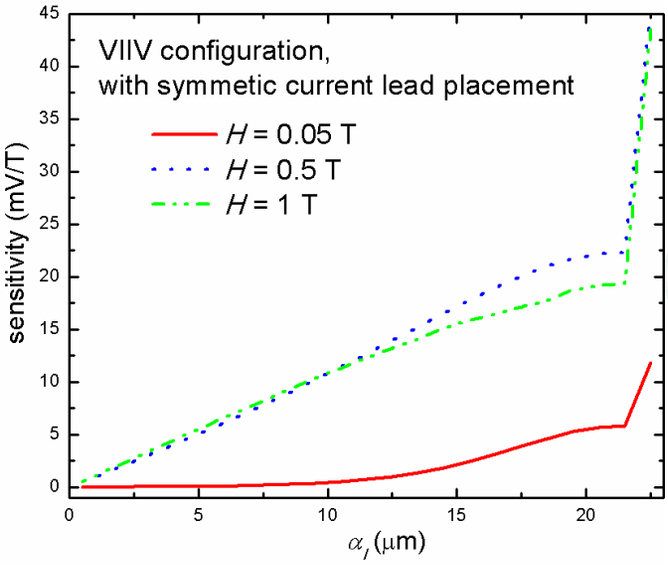

Figure 18. Sensitivity as a function of the placement of the current leads at various external fields for the EMR device with symmetric VIIV configuration.

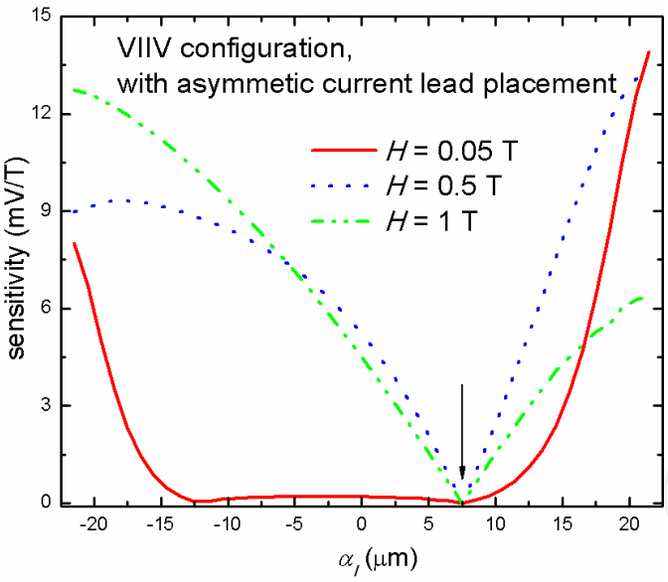

Figure 19. Sensitivity as a function of the placement of current leads at various external fields for the EMR device with symmetric VIIV configuration. The arrow indicates where the location of the fixed current lead.

The model was meshed with free triangular elements and consisted of approximately 6.8×10^5 elements and 1.4×10^6 degrees of freedom. The mesh density was varied adaptively.

The external magnetic field H of 1 T is applied in the positive z-direction to the model. The voltage output value of $V(H)$ between the probes V_1 and V_2 was evaluated and the EMR effect and sensitivity were calculated by the help of equation (18) and (19).

Figure 20 shows the distribution of the current density in devices with different contact resistivities at $H = 0$ T and $H = 1$ T. The current density is symmetric in case of $H = 0$ T whereas it is deflected by the Lorentz force at $H = 1$ T yielding increased density in the semiconductor and decreased density in the metal. With a low contact resistivity (10^{-8} Ω·cm^2), the current distribution in the device at zero and high fields are almost the same as in the ideal case with no contact resistivity. As the resistivity increases at the semiconductor/metal interface, it acts like a barrier and the current is increasingly inhibited to enter the metal shunt. Since the current density becomes larger in the semiconductor region, the value of $R(0)$ increases, thereby reducing the EMR effect. These dependencies can also be seen in Figure 21, which shows the current density distribution for the y/z-cross-section along the y-axis. It is worth to note that the area under each curve is identical to I. As the contact resistivity increases, the current density in the semiconductor increases, and a similar effect is obtained by increasing the magnetic field.

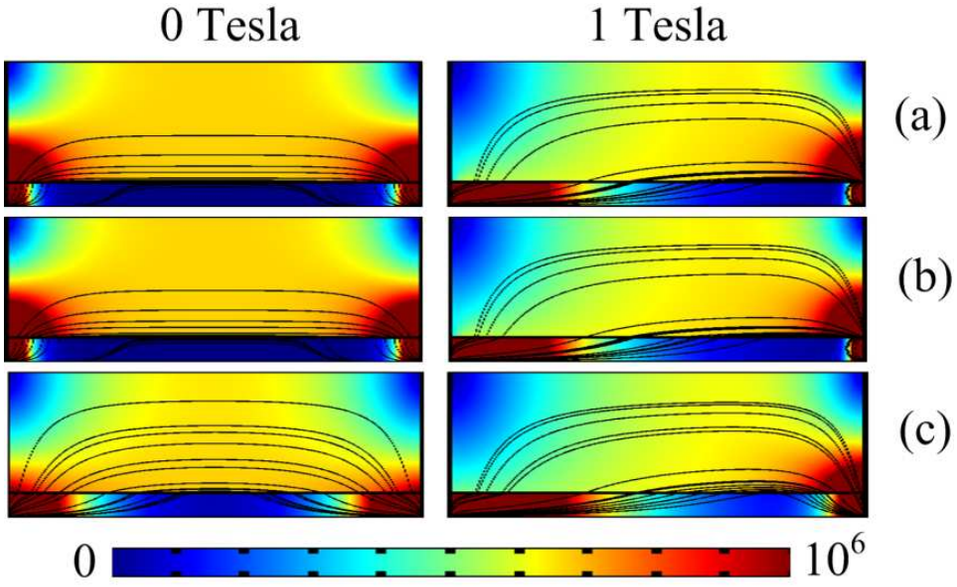

Figure 20. Current density distributions in different devices with various contact resistivities. (a) Ideal contact (no resistivity), (b) 10^{-8} Ω·cm^2, (c) 10^{-5} Ω·cm^2. The color bar represents the strength of the current density (A/m^2). Dark streamlines show the path of current. Left column: zero external field. Right column: external field is 1 T.

Figure 22 shows the EMR effect and the sensitivity as functions of the contact resistivities at $H = 1$ T. Nonlinear curve fitting is applied to find the exponential functions that approximate both the EMR effect and the sensitivity. For contact resistivities between 10^{-11} Ω·cm^2 and 10^{-7} Ω·cm^2, the EMR effect is almost constant. In case of the sensitivity, this range is from 10^{-11} Ω·cm^2 to 10^{-8} Ω·cm^2. As the contact resistivity increases beyond 10^{-7} Ω·cm^2 and 10^{-8} Ω·cm^2, the EMR effect and the sensitivity, respectively, decrease exponentially. In particular, a device with contact resistivity of 10^{-11} Ω·cm^2 shows an EMR effect of 1.1×10^5 %. The EMR effect is 1.1×10^6 % for the device with a contact resistivity of 10^{-8} Ω·cm^2 and it decreases to 6.0×10^5 % and 423 % for the devices with 10^{-6} Ω·cm^2 and 10^{-5} Ω·cm^2, respectively. The EMR effect is almost reduced by 95% compared to the ideal device (10^{-11} Ω·cm^2) when the contact

resistivity increases to 10^{-6} Ω·cm². Even in this case, the value is comparably high with an order of magnitude larger than values reported for contemporary GMR sensors. However, the EMR effect in the device with 10^{-5} Ω·cm² contact resistivity is only 0.4% of the one of an ideal device. For a contact resistivity lower than 10^{-8} Ω·cm², the sensitivity shows a value of app. 8.6 mV/T. It drops rapidly as the contact resistivity increases and has a value of 7.4 mV/T at 10^{-5} Ω·cm².

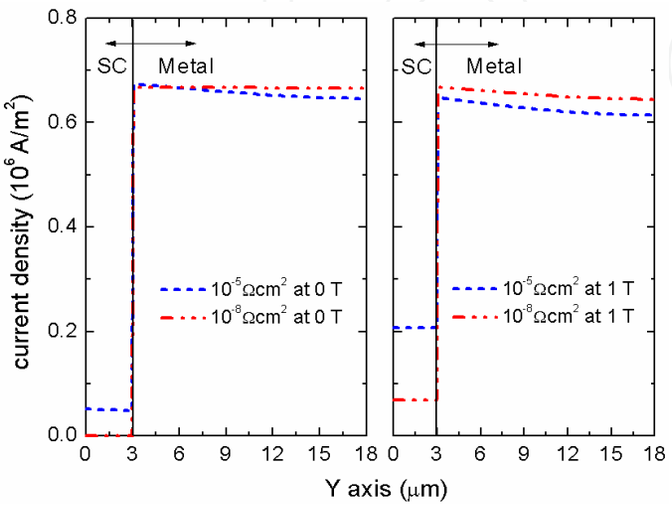

Figure 21. Current density distribution along the symmetry axis (y-axis) of the EMR devices with different values of the contact resistivity of the interface between semiconductor (SC) and metal at magnetic fields of (a) 0 T and (b) 1 T.

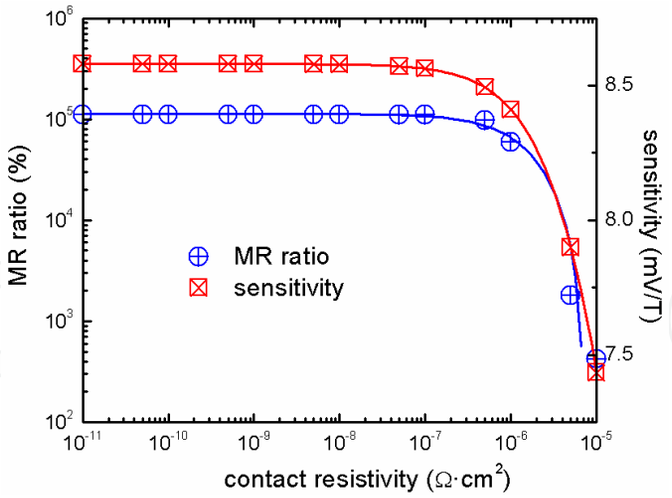

Figure 22. EMR effect and sensitivity as a function of the contact resistivity at 1 Tesla (MR ratio and contact resistivity axes are logarithmic).

8. Conclusion

In this chapter, we discussed the basic concepts of the Hall effect and EMR effect. We introduced a mathematical model to describe the inhomogeneous conductivity of a

conductor under the application of a magnetic field, which can be used to simulate both effects. The model is applicable for 2-D simulations as well as 3-D simulation. Especially for complex designs, the FEM is a convenient technique to carry out the simulation. While in case of Hall devices a 2-D simulation is normally sufficient, the structure of EMR devices requires a 3-D simulation in order to obtain accurate results. Specifically, for the EMR ratio we found an error of almost 30 % at 1T for the 2-D model and about 5 % for the 3-D model compared to experimental results. The model has been employed to simulate Hall and EMR devices. The focus of the chapter has been put on the investigation of EMR devices, since, compared to Hall devices, they have not been studied yet.

The modeled EMR device is of bar-type geometry since this is the most promising one for future applications taking into account device miniaturization and fabrication. The sensitivity of the device is investigated thoroughly, since it is the most significant parameter for many sensor applications and has not been addressed previously. Four different geometric parameters are investigated and the results show that an optimal performance requires certain aspects of the design to be customized for specific applications. The length/width ratio α of the semiconductor layer is found to have an optimal value between 10 and 20 for strong magnetic fields and 5 for weak ones. The placement of the voltage probes and current leads crucially influences the output sensitivity. In general, IVVI and VIIV devices are affected in a similar way. The two inner probes need to be placed as close as possible to the corners of the device in order to provide a high sensitivity. This leads to the surprising result that an EMR sensor with high sensitivity can be reduced to a two-contact device with the two contacts located at the corners of the semiconductor layer. An asymmetric arrangement of the contacts does not yield an improved performance at high fields, but has a positive effect on the low field sensitivity.

The simulations also show that the EMR effect and output sensitivity won't drop until the contact resistivity between the semiconductor and metal exceeds 10^{-8} $\Omega \cdot cm^2$. This result is consistent with experimental results reported previously. Interestingly, a device with contact resistivities up to 10^{-6} $\Omega \cdot cm^2$ still could show a considerable large sensitivity which is 95% of that in the device with contact resistivity of 10^{-8} $\Omega \cdot cm^2$. Attempts to reduce the contact resistivity below this value will not yield any further improvement of the performance of the device, which is often governed by the sensitivity. This is an important finding since, in practice; a good ohmic contact with low resistivity requires a costly device fabrication with carefully controlled material growth and a rapid thermal annealing process after the deposition of the material.

Author details

Jian Sun* and Jürgen Kosel

Physical Sciences and Engineering Division, King Abdullah University of Science and Technology, Thuwal, Kingdom of Saudi Arabia

* Corresponding Author

9. References

[1] Edwin H (1879) On a New Action of the Magnet on Electric Currents. American Journal of Mathematics. 2 (3): 287–292.

[2] Ramsden E (2006) Hall-effect Sensors: Theory and Applications. Oxford: Newnes.

[3] Solin S, Thio T, Hines D, Hermans J (2000) Enhanced Room-Temperature Geometric Magnetoresistance in Inhomogeneous Narrow-Gap Semiconductors. Science. 289: 1530-1532.

[4] Moussa J, Ram-Mohan L, Sullivan J, Zhou T, Hines D, Solin S (2001) Finite-Element Modeling of Extraordinary Magnetoresistance in Thin Film Semiconductors with Metallic Inclusions. Phys. Rev. B 64: 184410.

[5] Rowe A, Solin S (2005) Importance of Interface Sampling for Extraordinary Resistance Effects in Metal Semiconductor Hybrids. Phys. Rev. B. 71: 235323.

[6] Moussa J, Ram-Mohan L, Rowe A, Solin S (2003) Response of an Extraordinary Magnetoresistance Read Head to a Magnetic Bit. J. of App. Phys. 94(10): 1110-1114.

[7] Solin S, Hines D, Rowe A, Tsai J, Pashkin Y (2003) Nanoscopic Magnetic Field Sensor Based on Extraordinary Magnetoresistance. J.Vac. Sci. Technol. B, 21(6): 3002-3006.

[8] Moller C, Kronenwerth O, Heyn C, Grundler D (2004) Low-Noise Magnetic-Flux Sensors Based on the Extraordinary Magnetoresistance Effect. Appl. Phys. Lett. 84: 3343-3346.

[9] Solin S, Hines D, Rowe A, Tsai J, Pashkin Y, Chung S, Goel N, Santos M (2002) Nonmagnetic Semiconductors as Read-Head Sensors for Ultra-High-Density Magnetic Recording. Appl. Phys. Lett. 80(21): 4012-4014.

[10] Smith N, Arnett P (2001) White-Noise Magnetization Fluctuations in Magnetoresistive Head. Appl. Phys. Lett. 78(10): 1448-1450.

[11] Zhou T, Hines D, Solin S (2001) Extraordinary Magnetoresistance in Externally Shunted Van Der Pauw Plates. App. Phys. Lett. 78(5): 667-669.

[12] Holz M, Keronenwerth O, Grundler D (2003) Optimization of Semiconductor Metal Hybrid Structures for Application in Magnetic-Field Sensors and Read Heads. Appl. Phys. Lett. 83: 3344-3346.

[13] Hoener M, Kronenwerth O, Heyn C, Grundler D, Holz M (2006) Geometry-Enhanced Magnetoresistance of Narrow Au/InAs Hybrid Structures Incorporating a Two-Dimensional Electron System. J. Appl. Phys. 99: 036102.

[14] Hewett T, Kusmartsev F (2010) Geometrically Enhanced Extraordinary Magnetoresistance in Semiconductor-Metal Hybrids. Phys. Rev. B. 82: 212404.

[15] Sun J, Kosel J (2011) Finite Element Analysis on the Influence of Contact Resistivity in an Extraordinary Magnetoresistance Magnetic Field Micro Sensor. J. Supercond. Nov. Magn. DOI:10.1007/s10948-011-1256-8.

[16] Sun J, Gooneratne C, Kosel J (2011) Design Study of a Bar-Type EMR Device. IEEE Sensors Journal.12(5): 1356-1360.

[17] Zawadzki W (1974) Electron transport phenomena in small-gap semiconductor. Advances in Physics. 23: 435-522.

[18] Abeles B, Meiboom S (1956) Galvanomagnetic Effects in Bismuth. Phys. Rev. 101: 544–550.

[19] Zienkiewicz O, Taylor R, Zhu J (2005) The Finite Element Method: Its Basis and Fundamentals. Oxford: Elsevier Butterworth-Heinemann